Development of Graphene Oxide Nanosheets as Potential Biomaterials in Cancer Therapeutics: An In-Vitro Study Against Breast Cancer Cell Line

Yugal Kishore Mohanta[1] · Kunal Biswas[2] · Pradipta Ranjan Rauta[3] · Awdhesh Kumar Mishra[4] · Debashis De[5] · Abeer Hashem[6] · Al-Bandari Fahad Al-Arjani[6] · Abdulaziz A. Alqarawi[7] · Elsayed Fathi Abd-Allah[7] · Saurov Mahanta[8] · Tapan Kumar Mohanta[9]

Abstract

Recent advances in nanotechnology and nano biomaterials have attracted considerable attention in the field of cancer therapy. The development of biocompatible nanotherapeutics that selectively target cancer cells is a prime area of interest in current research. In the present study, graphene oxide nanosheets were synthesized using a modified Hummer's method and characterized by using FTIR spectroscopy, Raman spectroscopy, and X-ray Diffraction analyses, FE-SEM, HR-TEM and AFM. FT-IR spectra revealed the presence of the characteristic wave-numbers of 1585 cm^{-1}, 2841 cm^{-1}, and 3443 cm^{-1} uncovering the presence of intrinsic functional groups predominantly C=C, C-O, and C=O bonds. The characteristic intrinsic defect proportions in the as-prepared GO sheets exhibited a portion of the I_D/I_G ratio of ~ 1.05, indicating thereby a lesser proportion of available defect quantity in our synthesized graphene oxide sheets. XRD studies uncovered an interesting characteristic value of (001) and (002) lattice planes at a diffraction angle of 30°, which indicated a crystalline nature of the as-prepared graphene sheets. Thermo Gravimetric analyses of the as-prepared sheets indicated that in the range of 300–900 °C, the sheet exhibited a tremendous rate of thermal response at different applied temperatures, uncovering the underlying physico-chemical attributes of the sheets. It is observed from the DLS experimentation that GO sheets exhibited a zeta potential ζ-potential of − 9.3 mV, which is expected to be a most stable colloidal form. The lateral thickness of the graphene nanosheets was approximately 6.45 nm, which was corroborated by the TEM and AFM analyses, respectively. The potential biomedical application of graphene nanosheets was evaluated by assessing the cytotoxicity and antioxidant activity. The IC_{50} of H_2O_2 scavenging activity by GO sheets was determined to be 61.91 ± 1.14 µg/ml. The DPPH and H_2O_2 scavenging activity of the GO sheets increases with the increase with the dosage concentrations from 25 to 400 µg/ml, respectively. The in-vitro tests revealed that the GO sheets had a high level of cytotoxicity to the human breast cancer MDA-MB-231 cells

Yugal Kishore Mohanta, Kunal Biswas, Pradipta Ranjan Rauta, Awdhesh Kumar Mishra have contributed equally to this work.

✉ Yugal Kishore Mohanta
ykmohanta@gmail.com

[1] Department of Botany, Maharaja Sriram Chandra Bhanj Deo University, Baripada 757003, India

[2] Department of Biotechnology, Maulana Abul Kalam Azad University of Technology, West Bengal 741249, India

[3] Asian Institute of Public Health University, Bhubaneswar 751001, India

[4] Department of Biotechnology, Yeungnam University, Gyeongsan, Gyeongsangbuk-do, Republic of Korea

[5] Department of Computer Science and Engineering, Maulana Abul Kalam Azad University of Technology, West Bengal 741249, India

[6] Botany and Microbiology Department, College of Science, King Saud University, Riyadh 11451, Saudi Arabia

[7] Plant Production Department, College of Food and Agricultural Sciences, King Saud University, Riyadh 11451, Saudi Arabia

[8] National Institute of Electronics and Information Technology, Guwahati, Assam, India

[9] Natural and Medical Sciences Research Centre, University of Nizwa, Nizwa 616, Oman

that was concentration dependent. In contrast, the cytotoxicity of the GO sheets against the HaCaT normal cell line was marginal, suggesting that the graphene nanosheets could be safely used in cancer therapy.

Graphic Abstract
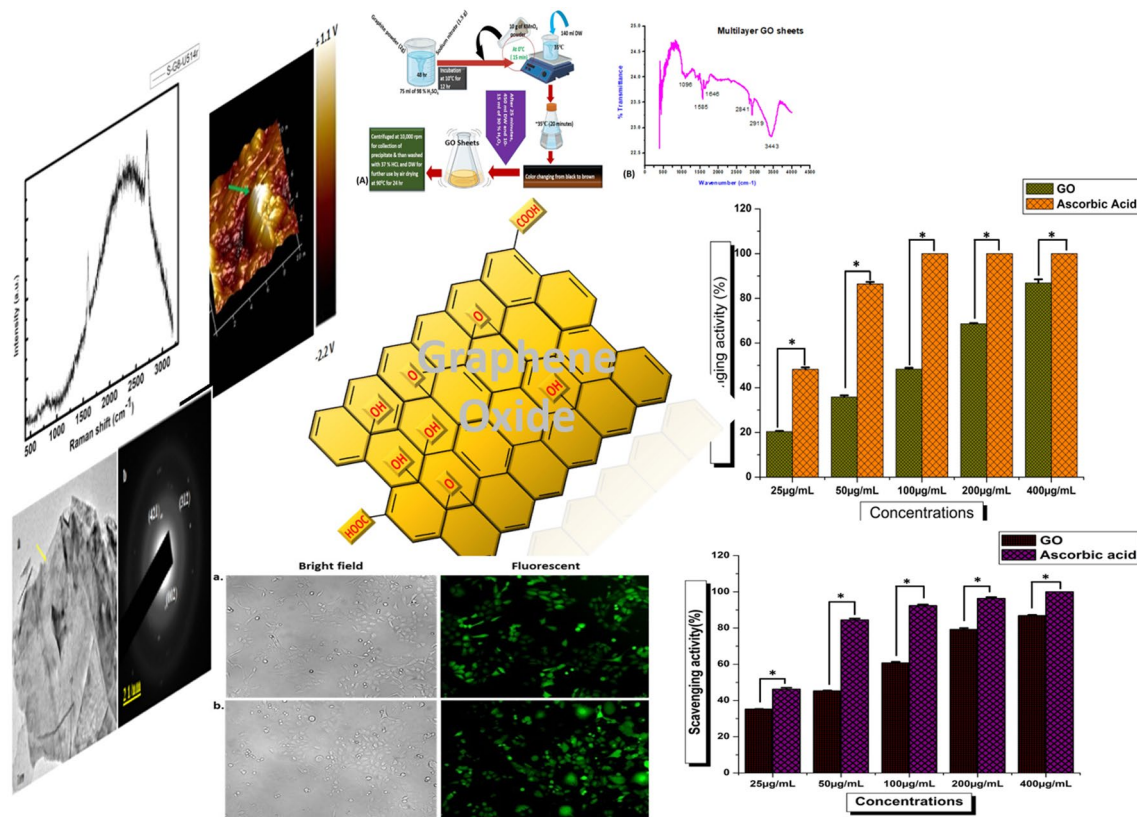
1 Introduction

The novel and fascinating properties of graphene-based materials suggest that these materials may have many potential biomedical applications [1, 2]. Graphene oxides are a class of nano-materials in the size range of 1–100 nm and fall into a category of two-dimensional carbonaceous nano-materials with dimensions of approximately a few nanometers in thickness. Owing to the unique physio-chemical properties of graphene oxide (GO), including the available surface oxygen groups, GO can form a stable suspension in different solvents, indicating its hydrophilic nature within the family of carbonaceous nanomaterials [3, 4]. Due to the presence of a unique surface to volume ratio, along with surface properties such as a huge concentration of surface atoms, augmented surface energy value, and other characteristics, makes GO a suitable candidate for a myriad of applications. Potential applications range from biomedical

applications (viz. drug delivery, protein therapy etc.) and bioengineering (biosensors and bioimaging) to anti-microbial therapy and bioengineering (scaffolding of tissue) [5, 6]. Due to its high surface to volume ratio, GO sheets provide a reactivity and adsorption platform for other biological macromolecules enabling bioprocesses to occur at a nanoscale level that are mesoscopic in nature [7]. The probability of redox reactions between the material and a biological system due to the free electrons present on the surface of graphene oxide sheets, increases the number of potential applications of carbonaceous nano-materials in biological systems [8].

Nanobiotechnology has emerged as a promising platform for employing nanomaterials in the field of cancer biology [7]. Due to the unique physio-chemical properties of the nanomaterials, the same could be used for targeted drug delivery for bearing the outcompeting behavior of natural delivery mechanisms such as reaching the nuclear membrane and penetrating it for delivery in the proteins and the DNA

sequences [5]. Graphene oxide [GO] has been recently proposed as a good agent in cancer therapeutics and diagnosis [9, 10]. The morphology and the viability of the glioma cells U87 and U118 respectively, have been shown to be less effective from the treatment of GO sheets [11]. Also, [12] has studied the adverse effect over the A549 cells due to the generation of oxidative stress by GO. It has also been reported that GO sheets bring significant damage to the mitochondrial membrane, resulting in altered mitochondrial potential [13]. Compared to other nano-scaled nanomaterials, such as gold and silver nanoparticles which are used in different medical therapies, carbonaceous materials like GO have lesser deleterious intrinsic activity in the drug delivery process of DNA, RNA for achieving targeted drug delivery mechanism [14–16]. Apart from, such graphene-based nanomaterials, several other combined organometallic nanomaterials are developed both physico-chemical and eco-friendly approach for potential biological and environmental applications [17]. Inspired from the research findings on the development of novel nanomaterials, the current GO nanomaterials with potential cancer therapeutic applications have been conceptualized [18–22]. Besides biomedical applications, these nanomaterials are technologically a very beneficial kind of materials for usage in environmental remediation and coating materials [23–28]. As a result, these materials are becoming immensely popular as novel tools in the biomedical field [29].

The surface properties of pristine graphene oxide and graphene sheets increases their overall potential for activity within biocompatible applications [30, 31]. In this regard, an interaction between GO sheets and targeted ligands in lung epithelial cells [32], neuronal cells [33] and fibroblast cells has been reported [34]. Furthermore, the use of GO sheets in conjunction with sulfonic acid in drug delivery systems makes the GO suspension more stable, while decorating the sheets with folic acid molecules has been used to target human breast cancer cells with folic acid receptors [35]. Folic acid-conjugated GO sheets have been employed for the delivery of anti-cancer drugs, such as doxorubicin and calprotectin, into tumor cell lines with great success in MGC803 cells [36]. Yang et al., [37] reported that a higher rate of uptake in tumor cells and in-vivo photothermal therapy was achieved by using PEGylated Graphene sheets in a mouse model subjected to an ultra-low power laser injection of 2 W cm^{-2}. The interaction of graphene with DNA/RNA macromolecules favors the use of GO sheets over GO alone, due to the presence of the carboxylic, hydroxide, and epoxy groups present in GO sheets, which provides greater potential bioactivity and thus, greater potential application in a wide range of biomedical fields and bio-macromolecular systems [30]. The higher rate of drug adsorption to hydrophobic materials also makes GO a preferred choice amongst the graphene family of nano-scaled materials, such

as graphene, rGO (large GO), and others [38]. Extensive studies of graphene-based materials for different biomedical applications have fostered nano-biomaterial development for practical use and commercialization. More studies on graphene are required, however, to achieve safe and effective commercial applications of this technology.

Considering the high rate of death rate in carcinoma that is a repercussion of the inadequacy of response to current therapy, there is a constant search for new targets and more efficient therapeutic materials, as well as unique avenue of therapy deliver to tumor cells [39]. Moreover, the combinatorial approach of numerous drugs administers higher healing efficacy than single one. The composed drugs consolidation with graphene-based nanocarriers has been recommended in cancer therapy [40, 41]. Graphene and derivatives have been suggested as nanocarriers in cancer treatment due to low toxicity to mammalian cells at low concentrations; but in high concentrations it can destroy the plasma membrane and prevent the cellular internalization. Thus, it is highly indispensable to investigate the standard nanomaterial concentration for adequate cellular internalization [42].

In this present study, the Hummers method, with some modifications, such as the use of sulphuric acid [H$_2$SO$_4$], and varying the Graphite: KMnO$_4$ ratio in the reaction mixture, was used to optimize GO production. The cytotoxic activity of the GO nanosheets against the MDA-MB-231 breast cancer cell line was also evaluated, along with its effect on a normal, HaCaT cell line. During the application of any foreign biomaterials, there is the potential of inducing oxidative stress. Therefore, the DDPH radical and peroxide scavenging assays were also conducted. Results of the study indicate that oxidation plays a key role in the activity of GO nanosheets in biological systems.

2 Materials and Methods

2.1 Preparation of GO Nanosheets

GO nanosheets were prepared using the commonly-used method described by Zaaba et al. [43]. Graphite powder was subjected to chemical exfoliation using a modified Hummer's method. Briefly, 1.5 g of sodium nitrate [MERCK, 98%] were mixed with 2 g of graphitic powder [Sigma Aldrich, 99.99]. The resulting powdered mixture was then placed in 75 ml of H$_2$SO$_4$ [Sigma Aldrich, 98%] and stirred for 48 h. The solution was then placed at 10 °C for 12 h, after which 10 g of KMnO$_4$ [Sigma Aldrich, 95%] powder was mixed in. The mixture was then placed in a 0 °C ice bath for 15 min. After this, the solution was heated to 35 °C on a hot-plate. Subsequently, 140 ml of deionized water [DI] was added to the solution during which time the exothermic

reaction occurring in the solution raised the temperature of the solution to ~98 ℃. The temperature of the solution was then lowered by placing the reaction solution in a 35℃-water bath for 20 min. The color of the solution began to change from black to brown, indicating that a chemical exfoliation process was occurring in the solution at a nano-scale level. After 25 min, 450 ml of DI water and 10–15 ml of H_2O_2 [Merck, 30%] was added to the solution. The solution then took on a yellowish hue, indicating the synthesis of GO sheets. The solution was then centrifuged and the precipitate was collected and washed with HCL [Sigma Aldrich, 37%], followed by a second washing with DI water. The pH of the solution was maintained at a pH of 7.0. The GO slurry was then poured into a fresh container for further use. The GO slurry was used to characterize the GO sheets and to prepare a dry powder by air drying the slurry in an oven at 90^0 C for 24 h.

2.2 FT-IR Spectroscopy

The FT-IR spectra of dried samples of GO sheets were identified and recorded using a Perkin-Elmer spectrum RX-1 IR spectrophotometer. The analysis of the GO sheets was performed by preparing the powdered samples into a KBr pellet [FT-IR grade, ≥99%] drying the pellet, and subsequently subjecting the dried pellet to ATR-attenuated FT-IR at 4500–500 cm^{-1}. Different functional groups against a specific inverse peak of wavenumber [cm^{-1}] were calculated to identify specific functional groups present in the structure of the GO sheets.

2.3 Raman Spectroscopy

The powdered samples of GO sheets were analyzed by Raman spectroscopy to identify any aberrant proportions in its structure by calculating the I_D/I_G ratio, which is a hallmark signature of any carbonaceous nano-materials. An Ar+ ion laser at an excitation wavelength of 514 nm was used and the vibrational modes of the intrinsic structures were studied using Lab Ram HR800 micro-Raman spectroscopy [Horiba Jobin-Yvon, France].

2.4 X-Ray Diffraction (XRD) of GO Sheets

The powdered samples were subjected to XRD [Bruker Advance D8] with a Cu Kα [$\lambda = 1.5406$ Å] to determine the crystalline structure and lattice planes in the material.

Different lattice planes against specific diffraction angles were calculated and used to determine the intrinsic details of the structure based on the diffractogram.

2.5 Field Emission Scanning Electron Microscopy (FE-SEM) of GO

The surface topography of the powdered GO sheets was observed using FE-SEM [EVO-60, Zeiss company]. The powdered samples of GO sheets were drop-casted on to the surface of a glass coverslip and dried overnight. The resulting samples were viewed under an FE-SEM at an operating voltage of 20 kV. The particle size of the GO sheets was calculated using a technique for determining the layer thickness and the particle diameter based on the use of a raster scanning mode.

2.6 High Resolution-Transmission Electron Microscopy (HR-TEM) of GO

For the HR-TEM analyses, the powdered samples were deposited on carbon-coated, copper grids [300 mesh size, regular grip, spi 2030 C] and allowed to dry overnight. The resulting samples were viewed in HR-TEM [FEI-TECNAI G2 2OS-TWIN, Netherland] at a frequency of 80 Hz.

2.7 Atomic Force Microscopy of GO

AFM [Bruker AXS Pte Ltd, Innova] was used to examine the surface properties of the GO sheets at a differential electrostatic charge distribution [in mV] using a cantilever-based deflection. The sample was prepared by drop-casting slurry onto a silicon wafer and allowing the samples to dry prior to examination by AFM.

2.8 Dynamic Light Scattering (DLS) of GO

The particle size and zeta-potential of the powdered GO sheets at room temperature were analyzed using a Zetasizer [Zs-90, Malvern, UK]. The dried samples were first adequately diluted in Phosphate Buffer Saline solution [0.15 M, pH 7.2]. Aliquots of the GO suspensions, at a concentration of 10 μg/ml from a stock [1 mg/ml], were subjected to further analysis under DLS. Particle size distribution was determined at a scattering angle of ~90 ℃.

2.9 Antioxidant Activity

The anti-oxidant potential of GO sheets was evaluated based upon a measurement of resistant DPPH free-radical scavenging. Briefly, 1.9 ml of a methanol solution of DPPH [Sigma Aldrich, 0.004%], and 0.1 ml of different concentrations of GO, were mixed together. The solution was then mixed robustly and kept for 30 min in the dark. Absorbance of the solution at 517 nm was then determined by using a Shimadzu UV-1280 spectrophotometer. The addition of
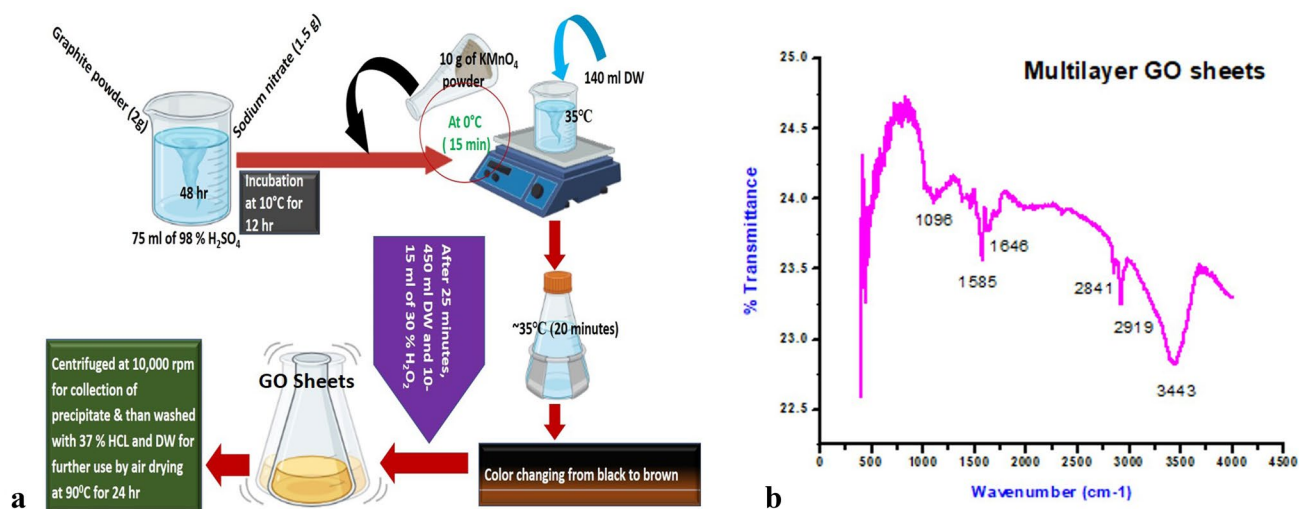
Fig. 1 **a** Synthesis of GO nanosheets. **b** FT-IR of graphene oxide nanosheet

ascorbic acid to DPPH was used as a control. All tests were performed in triplicate. The ability to scavenge DPPH radicals was calculated by using the following Eq. (1):

$$Ability\ avenge\ DPPH\ [\%] =\ [AO - A1]AO \times 100 \qquad (1)$$

In the equation, AO is the absorbance of the control, while A1 is sample absorbance.

H_2O_2 scavenging activity of the GO sheets was also determined using a slightly modified Ruch Figure method [16]. Briefly, a 40 mM H_2O_2 solution was prepared in KH_2PO_4-K_2HPO_4 [Sigma Aldrich, 0.05 M] phosphate buffer [pH 7.4]. Various concentrations of GO were then added to the prepared H_2O_2 solution (1.4 ml phosphate buffer and 0.6 ml 40 mM H_2O_2). The absorbance of the H_2O_2/GO solution was then measured after 10 min at 230 nm using a Shimadzu UV-1280 spectrophotometer, and used to estimate the concentration of H_2O_2. Ascorbic acid, instead of the GO solution, was used as a positive control. All tests were performed in triplicate and H_2O_2 scavenging ability was calculated by using Eq. [1].

2.10 Cytotoxicity and Biocompability with Different Cell Lines

2.10.1 Cell Culture

The cell lines chosen for the cytotoxicity assay were a human skin HaCaT and a breast cancer cell line [MDA-MB 231]. The basal medium used for all cell culture experiments was Dulbecco's Modified Eagle's medium [GIBCO™ USA] supplemented with 10% Fetal Bovine Serum [GIBCO™ USA] and streptomycin sulfate and benzyl antibiotics [Sigma Aldrich, ≥ 96%] at a final concentration of 100 µg/ml and
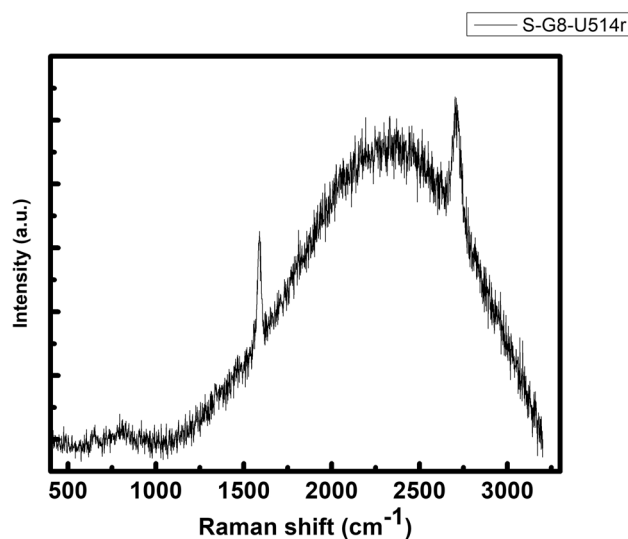

Fig. 2 Raman spectroscopy plot of graphene oxide nanosheet

100 U/ml, respectively. Cell cultures were maintained at 5% CO_2 and 37 °C throughout all the experiments. The cells were passaged using 0.25% Trypsin-EDTA [GIBCO™ USA] at around 80% confluence. Cells were seeded in 96-well plates at a density of 5×10^3 cells/well for the MTT assays.

2.10.2 MTT Assay

Cytotoxicity and biocompatibility were assessed using an MTT colorimetric assay at 24 and 48 h after incubation of the cell lines with the GO nanosheets [44]. Doxorubicin [Sigma Aldrich, 98.0–102.0%] was used as a positive control. A stock solution of dimethyl thiazolyl-diphenyltetrazolium bromide [MTT; 1 mg ml^{-1}] in PBS was prepared

immediately prior to use. A 500 μl volume of the MTT solution [50 μg ml^{-1} MTT in culture medium] was added to each culture dish without a cover. Cells were incubated for 3 h, and reduced formazan was then extracted with 500 μl DMSO and absorbance was measured at 570 nm in a spectrophotometer. Cell survival was expressed as the percentage of absorption of treated cells in comparison with untreated, control cells.

2.11 Statistical Analysis

Each assay was performed in triplicate to ensure reproducibility. The results of the antioxidant assays were expressed as a percentage of inhibition, while the cytotoxicity results were expressed as percent viability, relative to the control. Values obtained in the antioxidant and cytotoxicity assays for the different treatment groups vs. the controls were statistically evaluated using a Student's t-test ($p \leq 0.05$).

3 Results and Discussion

3.1 Characterisation of GO Sheets

3.1.1 Fourier Transform Infra-Red Spectroscopy

The GO nanosheets were evaluated prior to their use in the in vivo bio-application studies. The structure and possible function of individual molecules were evaluated to better link activity of the GO nanosheets with its structural components. Prior knowledge of the molecules and bonding pattern could also help to predict expected outcomes in the use of the GO nanosheets. The FT-IR spectra of the architecture of GO sheets (Fig. 1b) revealed the presence of the characteristic wave-numbers of 1585 cm^{-1}, 2841 cm^{-1}, and 3443 cm^{-1}. These wave numbers represent the functional groups linked to the structure of the GO sheets, and reveal the presence of C=C, C-O, and C=O bonds, respectively. The wave number present at ~ 1096 cm^{-1} is associated with

both C-C and C-O bonds. The broad signal observed around 3443 cm^{-1} indicates the O-H bond vibration of the hydroxyl groups present in the GO architecture [45]. Such vibrational peaks indicate the pristine architecture of the carbonaceous skeleton of the as prepared GO sheets similar to the previous findings [46]. Such interesting findings denotes the major oxygenated functional groups associated with the formation of the as synthesized GO sheets during bottom-up fabrication of GO sheets from its native precursor Graphite with several interplay of reducing and oxidizing agents. Our findings are broadly in closer proximity to the recent findings in one of such studies where the influence of KMN0$_4$ has been ascertained over the synthesis of GO sheets in a typical bottom-up laboratory preparation of GO thin sheets.

3.1.2 Raman Spectroscopy

Raman spectroscopy is an important analytical tool that provides both qualitative and quantitative data on nanomaterials based on its chemical composition and structure [47]. The Raman plot (Fig. 2) contains the I_D/I_G ratio of ~ 1.05, which is characteristic of powdered GO sheets. The defect ratio represents the compromised proportion and lesser quantified nature of the available defects present in the GO sheets. More specifically, it indicates the presence of a slightly lower number of dangling bond associations in the native structure of the GO sheets, compared to the previously reported graphene sheets of rGO forms that have a value of 1.35. Such observations indicate a more conductive nature for GO forms, relative to its other counterparts [Graphene, rGO, etc.], making it suitable as an inhibitory anti-cancerous agent that can be used against a variety of cancer cells. Further, from the Raman analyses it is becoming evident the nature of the symmetry of the available D and G bands, which in returns dictates the formation of the defects associated with the synthesis of the GO sheets. Such defected symmetry is mainly occurring due to the presence of available sp2 hybridization of the carbon architecture in the GO sheets [48]. As it has been reported previously [48]

Fig. 3 **a** XRD spectroscopy plot of graphene oxide nanosheet; **b** TGA of GO sheets
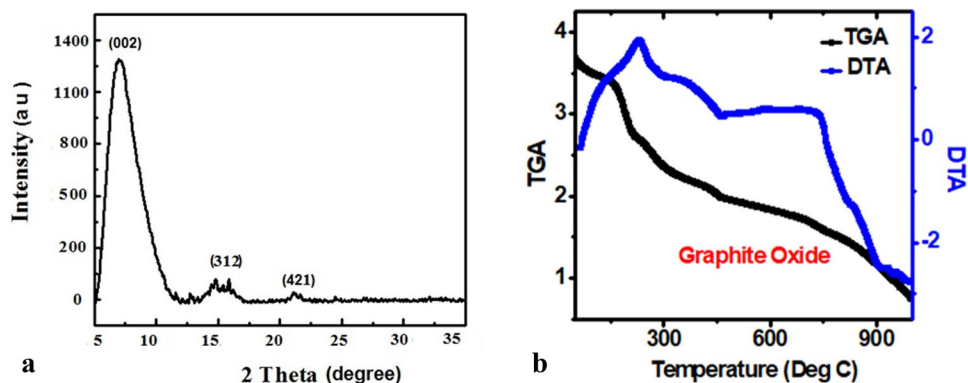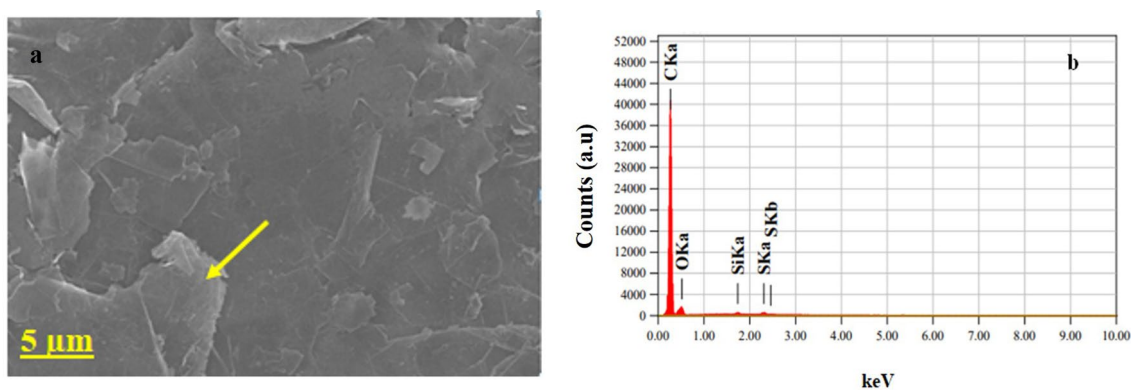
Fig. 4 **a** FESEM and **b** EDAX of graphene oxide nanosheet

that G band peak refers to the symmetry of the carbon atoms whereas D band peak refers to the disorder induction in the available carbon atoms [49, 50]. In our findings there seems to be occurrence of lateral shifting in the ID/IG ratio, which is mainly due to the graphitic exfoliation taking place during oxidizing effect of KMN0₄ reagent. The shifting in the defect ratio and proportions is also in corroboration with the rising oxidizing level owing to the disruption in the graphitic stacking order [51].

3.1.3 X-Ray Diffraction

The X-Ray Diffraction [XRD] analysis (Fig. 3) revealed the presence of lattice planes that are characteristic for powdered GO sheets. Notably, (001) and (002) lattice planes at a diffraction angle of ~ 10° were evident. These characteristic lattice planes indicate the nature of the available crystallinity of GO sheets. The polycrystalline nature of GO sheets is evidence that such lattice planes are present and were corroborated by the TEM SAED pattern. It is usually noticed from the X-Ray Diffraction studies that different phase purity of the synthesized GO sheets at the different amount of KMNO₄ reagent as oxidizing agents [46]. The differential peak of lattice planes as evident from the Fig. 3, is mainly

because of the incomplete rate of oxidation of the Graphitic flakes upon subjection to the oxidizing agents [52]. The crystalline lattice planes at around (002) demonstrates the formation of well-ordered crystalline nature of the GO sheets in the synthesis process. The studies explain the interlayer spacing distance of 0.19 nm, which is in parity with previous findings [46]. It could be understood that the rate and type of crystalline lattice formation of GO sheets is mainly dependent upon the oxidation level of the GO films by the oxidizing agents.

Thermo-gravimetric analysis (TGA) is a method of thermal analysis in which the physical and chemical properties of materials are measured as a function of increasing temperature (with a constant heating rate), or as a function of time (with constant temperature and/or constant mass loss). TGA contrasts with DTA, where the material under study and an inert reference undergoes identical thermal cycles, and differences in the temperature between a sample and reference are recorded [53]. The results indicated that exposing the as-prepared GO materials to temperature changes affected its physico-chemical properties with time. The physico-chemical properties of the GO sheets were altered by changes in temperature and defects were induced in the structure of the material, which was corroborated by the

Fig. 5 **a** h-TEM of graphene oxide nanosheets; **b** SAED of GO sheets indicating crystalline lattices
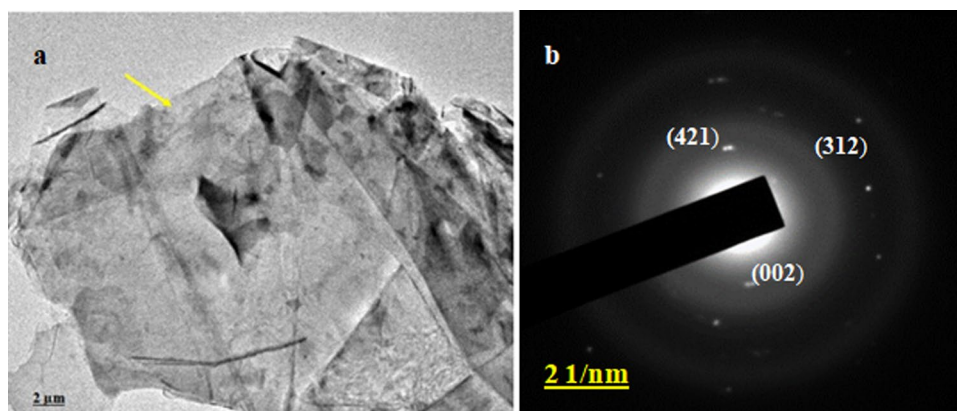
Raman defect ratio (I_D/I_G) of the material. The changing thermal losses with the increasing temperature range from 300–900℃ shows the dynamical response of the GO sheets underlying physico-chemical properties which is dependent upon the thermal kinetics of the system. It is understood that with the subjection of the thermal exposure, the available C-C bonds starts to jiggle, resulting into a thermodynamical change in the interlayer of the GO sheets, causing a resultant TGA plot as shown in Fig. 3b. Such studies aids in uncovering the impact of changing temperature over the GO sheets which would enable to understand the percentage of weight loss (mass) [54] of the GO material and its associated volatile components with the constant rate of heating exposure in a period of time.

3.1.4 FE-SEM Analysis

Field emission scanning electron microscopy provides information on the surface topography and composition of nanoscale materials [53]. Data on the surface morphology is highly useful regarding the potential use of the nanomaterials in medical devices and for other applications. The typical surface topography of GO sheets was evident in the FESEM analysis (Fig. 4). Surface undulations were evident in GO sheets (Fig. 4A), as well as rough edges. Undulations and rough edges are the result of reaction kinetic phenomenon resulting in reduction and oxidation processes during the production of the GO powders. Energy Dispersive X-Ray Spectroscopy (EDAX or EDS) at a characteristic energy (keV) was used to evaluate the intrinsic chemical constituents of the as-prepared GO sheets (Fig. 4b). As evident in Fig. 4B, carbon (C) and oxygen (O) make up the major proportion of the as-prepared GO sheets. The EDS results indicate that during the synthesis of the GO sheets from its precursor graphite compound, various reducing agents and other chemical constituents used in its preparation, as well

as solvents such as H_2SO_4, are present as trace amounts of Sulphur (S), while the traces of silicon (Si) been originated from the silicon substrate of the grid used to examine the GO sheets in the FE-SEM. It could be noticed from Fig. 4a that the implications of oxidizing agents over the GO surface is clearly evident as more crumpling in the surface properties which could be easily seen from the figure. Our findings are in strong agreement with the previous literature [55], where the implication of $KMNO_4$ as oxidizing agent and other reagents involved during the synthesis procedure is seen. The formation of clear crumpling nature over the surface of the GO sheets is an indication that perfect exfoliation of graphite precursor has been taken place which resulting into deformation process during exfoliation and simultaneous restacking process taking place during the synthesis procedures which is in agreement to the previous findings [55].

3.1.5 HR-TEM Analysis

The primary purpose of the High Resolution-Transmission Electron Microscopy (HR-TEM) analysis was to observe high magnification images of the internal structure of the GO sheets and gather information related to the crystalline structures, internal fractures, stress, and contamination of the test sample. Information on the internal structure allows one to have greater confidence in the potential application of the nanomaterial and predict potential effects on the target system [56]. HR-TEM observations indicated that the internal structure of the prepared GO sheets possesses a folded morphology (Fig. 5). The presence of undulating folds and rough edges in the carbon sheets are evidence of the successful synthesis of GO sheets as previously noted by several authors. HR-TEM imaging enables one to visualize the internal, structural architecture of the prepared GO sheets, which is not possible by FE-SEM. In contrast, HR-TEM provides a clear picture of the internal structure of GO sheets at a resolution of 2 microns. The layers of the GO sheets, resulting from the reduction and oxidation processes occurring during GO synthesis, can be readily seen in Fig. 5. The lateral thickness of the GO sheets was ~9 nm. Selected Area Electron
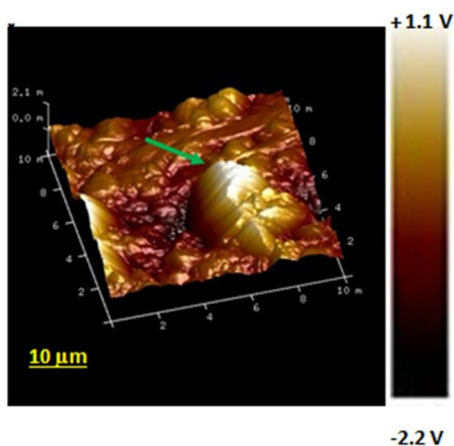

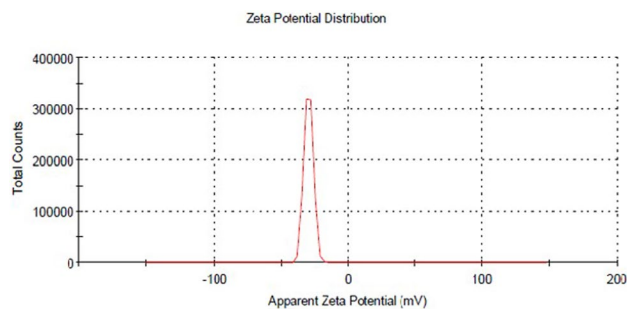**Fig. 6** AFM of graphene oxide nanosheets

Fig. 7 DLS of graphene oxide nanosheets

Diffraction (SAED) is an attachment to HR-TEM system of imaging that provides information on the underlying crystalline properties of the examined samples. SAED analysis of the powdered GO sheets revealed the characteristic polycrystalline nature of the samples (Fig. 5b). The results of the SAED analysis are in agreement with the results obtained in the X-ray Diffraction (XRD) analysis, both of which have revealed the polycrystalline structure of the GO sheets, due to its crystalline lattice planes (Fig. 3). Thus, SAED studies complement X-ray Diffraction studies for the examination of GO nanomaterials. The relative crumpling nature which is an indication of the successful formation of the GO sheets is clearly seen from Fig. 5a. It is clearly understood that such folded architecture bears a more robust rate of electronic conductivity in its layered structure, which is thought to be the responsible cause of the elicitation of the penetrating cell inhibiting activity when subjected to *in-vitro* cell lines. It is further anticipated that when the GO films bearing such rough edges comes into contact with the soft membraned cell systems like cancer cell lines, there undergoes an interplay of relative charge transfer mechanism between the tip of the GO films and the outer layered charged membrane resulting thereby a formation of electrostatic interaction making the cells susceptible to GO ingestion and thereby causing the cellular dis-integrity and damage.

3.1.6 AFM Analysis

In the application of a nanoscale material in living systems, local properties of a sample, such as height, friction, and magnetism, should be carefully assessed. The atomic force microscopy (AFM) analysis conducted in the present study
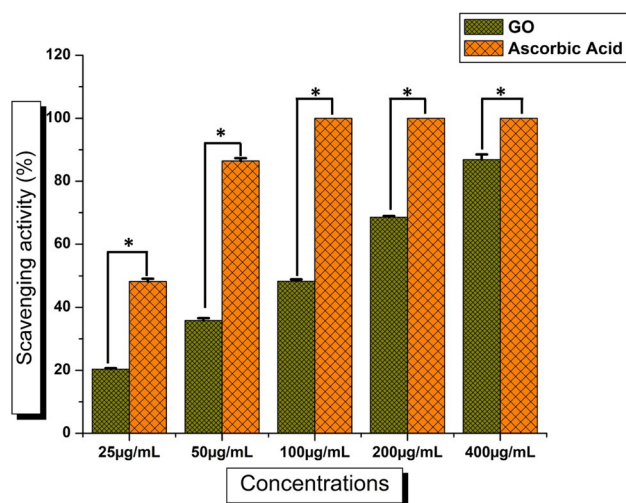

Fig. 8 DPPH radical scavenging assay of graphene oxide nanosheet. Error bar represents standard deviation of mean. *p ≤ 0.05. Significant difference (p ≤ 0.05) within a parameter between two lines is denoted by asterisk

Fig. 9 H_2O_2 radical scavenging assay of graphene oxide nanosheet. Error bar represents standard deviation of mean. *p ≤ 0.05. Significant difference (p ≤ 0.05) within a parameter between two lines is denoted by asterisk

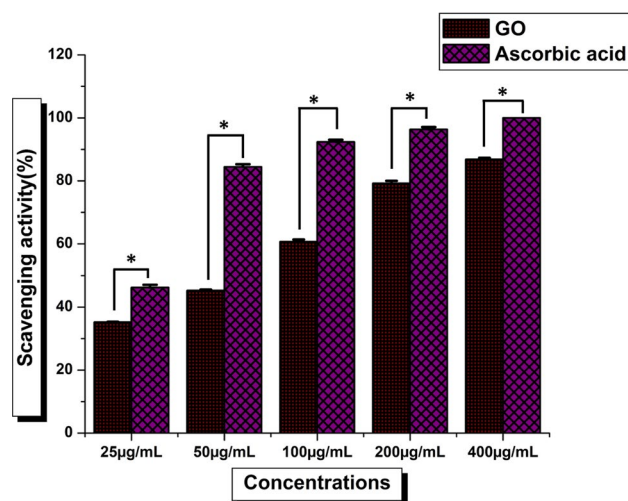provided information needed to determine its suitability for use in different bio-applications. Rough undulations at different tapping voltages of the AFM tip can be observed in Fig. 6. The thickness determined by AFM was in agreement with the results obtained in the HR-TEM analysis of the GO sheets. The charge distribution of the sheet at different electrostatic voltages is indicated by the colored bar graph. It is contemplated that as evident from the AFM images, the differential charge distribution in mV for the GO films causes a net interaction with the cellular membrane resulting into membrane rupture of the cancer in-vitro cells. Topologically, the 3D micrograph of the GO films (Fig. 6) makes it a clear impression that due to the use of oxidizing and reducing agents involved in the bottom-up synthesis of the GO sheets, there is an observation of irregular peaks and strains noticed in the micrographs. Such un-even exfoliated architecture which is in corroboration with the TEM images, indicates a better chance of cell inhibiting activity when tested into different soft biological systems *in-vitro*.

3.1.7 DLS Measurements of ζ-Potential

GO exhibits a ζ- potential of -29.3 mV, which is thought to be the most colloidal stable form (Fig. 7). An augmented cytotoxic effect against cancerous cells is observed by GO sheets due to its surface anionic charge. The percolation tendency of GO sheets may be attributed to the average size and overall tension occurring in the membranes of cancerous cells, which ruptures the membrane and allows entry of the material into the cell [57]. Endocytosis appears to be the prime mechanism underlying the entry of GO sheets into cells, however, further validation is required to confirm

Fig. 10 Fluorescence and bright field images of GFP-tagged MDA-MB-231 cells showed internalization of GOs at different time intervals; **a** Control MDA-MB-231 [10 ×], **b** GO treated MDA-MB-231 after 48 h [10 ×]
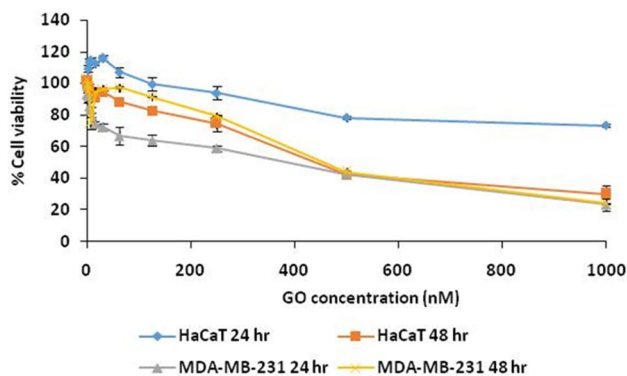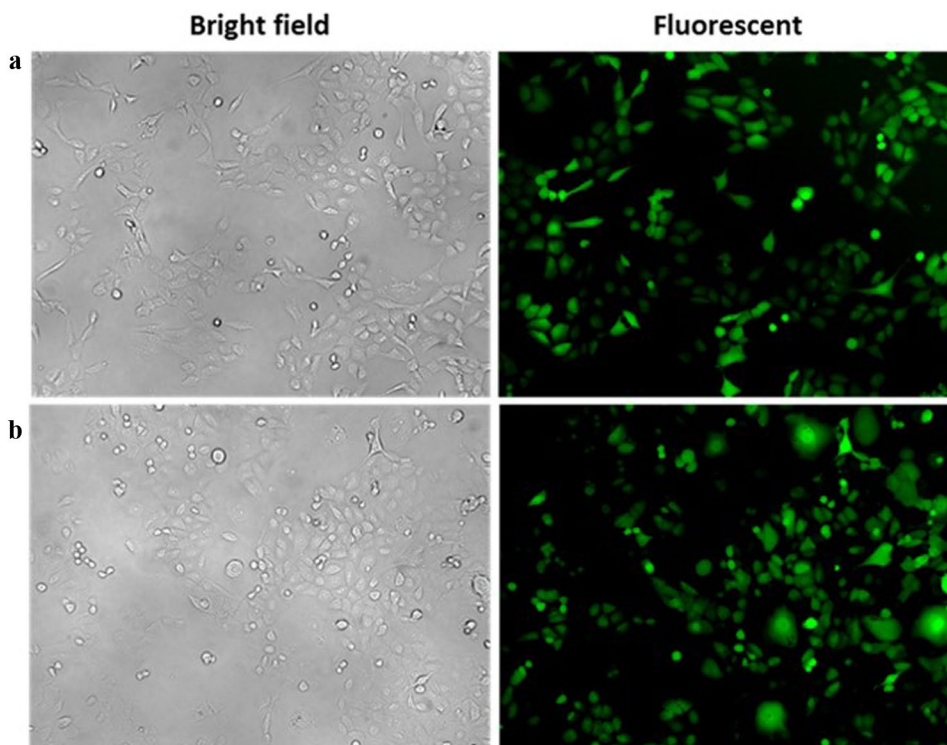

Fig. 11 Cell viability of MDA-MB-231 and HaCaT after treatment with different concentrations of GO nano formulations after 24 and 48 h

the mechanism by which GO sheets enter and exit living cells [58]. The interface of GO sheets with biological cells is also attributed to the electrical disruptions that occur at the material-bio interface. In this regard, the dimensions, size, shape, and intrinsic chemical composition of GO sheets play a significant role in the net cytotoxicity of the nanoparticles in biological systems [59].

The DLS analysis was repeated three times and a statistical significance of $p \leq 0.05$ was achieved for the repeatability of the experiments using a student's- t test. Colloidal stability of the GO was observed, which determines the surface

charge of the powdered GO sheets. The average colloidal stability of the material was determined to be ~ 29.3 mV.

The experimentation has been repeated thrice and the statistical significance of $p \leq 0.05$ has been achieved for the repeatability of the experimentations using students- t test. Colloidal stability has been observed in this study which determines how much is the surface charge existing over the powdered sample when experimented. The average colloidal stability of the material came to be ~ 29.3 mV upon triple repetition of the experimentation. It is clearly understood that the GO films of differential particle distribution and colloidal stability makes it a potential candidate for the net electrostatic interaction between the material and the cellular architecture. The colloidal stability also enables to understands the materials thermodynamical free energy associated with its intrinsic atomic configuration which makes it a suitable biomaterial when tested into different biological systems safely.

3.2 Anti-oxidant Assays

As indicated by previous studies, there are various types of nanoparticles that can function in free radical scavenging and act as antioxidant agents [60, 61]. The antioxidant properties of the prepared GO sheets were analyzed using the DPPH radical scavenging assay and an H_2O_2 assay. Results indicated that the free radical scavenging activity of GO sheets was concentration dependent (Fig. 8), with

Fig. 12 Cell viability assay of **a** GO treated MDA-MB-231 cell lines [24-hour post incubation] and **b** GO treated MDB-MB-231 [48-hour post incubation]
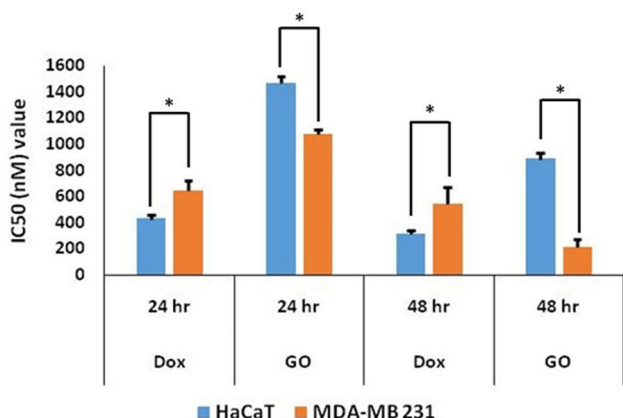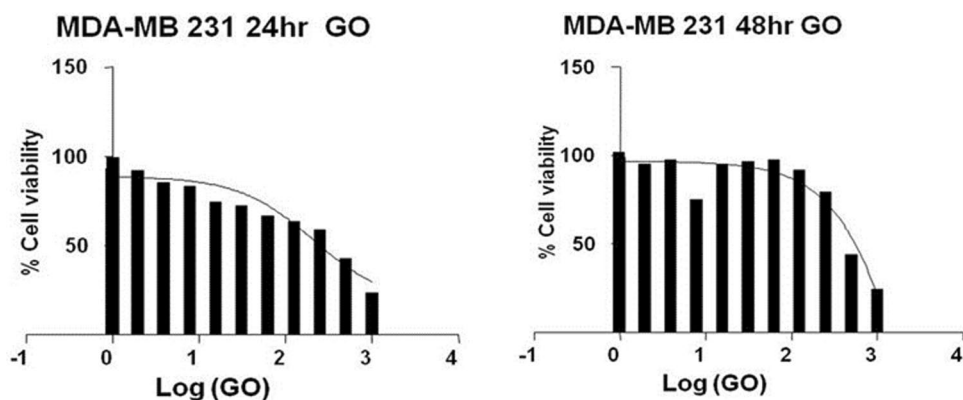

Fig. 13 Cell viability [IC 50 value] of MDA-MB-231, HaCaT, after treatment with different nano formulations [Dox: Doxorubicin [control], GO nanosheets] after 24 and 48 h. Error bar represents standard deviation of mean. *$p \leq 0.05$. Significant difference ($p \leq 0.05$) within a parameter between two lines is denoted by asterisk

scavenging activity increasing as the concentration of GO sheets increased from 25 to 400 µg/ml. The IC_{50} value was 105.82 ± 1.78 µg/ml. The mechanism of DPPH radical scavenging is achieved by the donation of hydrogen to the free radical s [62]. H_2O_2 radical scavenging activity was concentration dependent (Fig. 9). The IC_{50} of H_2O_2 scavenging activity by GO sheets was determined to be 61.91 ± 1.14 µg/ml. The intrinsic cytotoxicity of H_2O_2 is due to the release of OH- as H_2O_2 is not in itself reactive in nature. Therefore, any treatment regime employing the H_2O_2 assay needs to be carefully examined when dealing with the interface with biological systems, specifically liver cells *in vitro*. The use of a graphene-based treatment [graphene, rGO, and GO] in the biological systems helps to counterbalance the free radicals generated as a side effect of the peroxide assay in biological systems. This needs to be taken into account when measuring cytotoxicity and antioxidant activity of graphene-based compounds in biological systems. The antioxidant activity of GO sheets is based on the overall physico-chemical

properties of the GO materials [63]. The formation of the radical adduct at the sp^2 carbon sites determines the antioxidant activity of carbonaceous nanomaterials. The minimization of free radicals generated in H_2O_2 assays is also mediated by the formation of the second adduct leading to the donation of free radicals and a chelation system, thereby inhibiting the Fenton-based free radical system making GO-based antioxidant activity more prominent and significant [61, 62]. Based on the results of the DPPH and H_2O_2 assays, it appears that the GO nanosheets are safe for the development and use of biocompatible nanomaterials for different healthcare applications.

3.3 Microscopic Studies of GO Invasion

The cellular uptake of GO nanosheet was studied using fluorescent protein [GFP] tagged-MDA-MB-231 cells (Fig. 10). The cells were treated with 100 µg/mL of GO for a period of 48 h, after which the cells were visualized under a flour's fluorescence inverted microscope. The analysis of microscopic images indicated that the clusters of nanoparticles appeared in close vicinity to and in the cytoplasm of GFP-MDA-MB-231 cells and was passively absorbed into the cells in a time-dependent manner.

3.4 Cell Viability Assay

The HaCaT cells were treated with GO sheets in culture at varied concentration (0.97 nM to 1000 nM) for 24 h at 37^0 C. The methyl thiazolyl diphenyl-tetrazolium bromide [MTT] assay was used to evaluate Human keratinocyte (HaCaT) cell viability upon treatment with GO nanosheet (Fig. 11). The concentration dependent effect of GO sheets on HaCaT cell viability was observed from assay results. HaCaT cells exposed to 125 nM GO exhibited 99.26% level of cell viability. The viability percentage, however, slowly decreased as the concentration of GO increased. Exposure to 1000 nM GO reduced cell viability of HaCaT cells to,

73.43%. These results confirm that GO is relatively non-toxic to normal cells as more than 50% of the cells were viable, even at a higher concentration. Therefore, it appears that GO nanosheets can be used for various potential biological applications due to its biocompatibility property. The biocompatibility of GO with HaCaT cells has also been previously demonstrated in earlier studies [64].

The cell viability of GO treated breast cancer cells [MDA-MB-231] was accessed in a similar manner. In contrast to results with normal cells (HaCaT), the cytotoxicity assay of GO sheets with breast cancer cells [MDA-MB-231] revealed significantly higher levels of cytotoxicity (Figs. 12 and 13). The treatment of the cancer cells with a ~ 1000 nM GO sheets for 24 h decreased cell viability to ~ 23.46%. A time-dependent and dose-dependent cytotoxicity of GO nanosheets against MDA-MB-231 cells have been previously reported [65, 66].

The percentage of viable cancer cells were decreased as the concentration of GO increased. The percentage of viable cells were 63.82 and 92.04% after treatment with 125 nM and 1.95 nM GO solutions, respectively. These results indicate that MDA-MB-231 cells exhibit a concentration dependent response in cytotoxicity. The cytotoxicity, however, did not appear to be time-dependent as a similar percentage of viable cells were observed after both 24 and 48 h of incubation with the same concentration of GO sheets (Fig. 9). It is suggested that ROS production plays a measure role in the mechanism of cellular toxicity of GO sheets in human breast cancer cells [MDA-MB-231] [66]. GO toxicity in cellular systems is also determined by the biologically essential organelle, the mitochondrion, and the ROS that is generated and induces cellular apoptosis when a material, such as GO sheets, are introduced into a cell and disrupts metabolism [65]. In the case of treatment with doxorubicin [control], the IC50 values are higher in MDA MB 231 cells than HaCaT cells after both 24 and 48 h of exposure. In contrast, the IC50 values for the GO treatment were significantly lower in MDA MB 231 cells than in HaCaT cells after both 24 and 48 h of exposure (Fig. 13).

4 Conclusions

The present study demonstrated the impact of GO sheets on the viability of breast cancer cells. It was shown that due to the rough edges, and the lesser number of available defects in the structure of the GO sheets, the level of cytotoxicity towards the cancerous cells was very strong. GO sheets have exhibited an architectural skeleton of C=C, C-O, and C=O bonds. , a polycrystalline morphology bearing predominant (002) diffraction peaks at incident angle of $\sim 10^0$ as evident from the X-Ray Diffraction analyses. The obtained GO sheets exhibited an intrinsic lesser I_D/I_G ratio possessing lesser quantifiable defect proportions

of ~ 1.05, which is much lesser as compared to previously published work of ~ 1.35, making it thereby a potential and biocompatible carbonaceous material to be used in bio-systems for achieving an augmented therapeutic efficacy. The morphology and surface properties of the as-prepared GO sheets also supports the successful formation of lateral thickness of ~ 9nm, with colloidal net stability of ~ 29.3 mV, indicating a thermodynamically more stable form of GO sheets as compared to previously reported cases. The morphology of the treated cells was also altered upon GO solution exposure at different dosages, as when compared to the untreated cells, indicating that the cancer cells had been damaged by the GO treatment. GO-based treatment of cancerous cells demonstrates the extreme potential and capabilities of employing nanomaterials as an effective carbon-based anti-cancerous agent in the treatment of dreaded life-threatening diseases like cancers.

Author Contributions YKM and PRR were involved in the synthesis of GO nanosheets, antioxidant & MTT assays, and the preparation of the manuscript. KB, AKM, DD helped in the characterization of GO and drafting the manuscript. AH, AFA AAA, and EF revised the manuscript, SM analyzed the data and revised the manuscript, TKM drafted and revised the manuscript. All the authors read and approved the final manuscript.

Declarations

References

1. F. Tonelli, V. Goulart, K. Gomes, M. Ladeira, A. Santos, E. Lorençon, L. Ladeira, R. Resende, Graphene-based nanomaterials: biological and medical applications and toxicity. Nanomedicine **10**, 2423–2450 (2015)
2. K. R. D. Kasibhatta, I. Madakannu, I. Prasanthi, Hetero atom doped graphene nanoarchitectonics as electrocatalysts towards the oxygen reduction and evolution reactions in acidic medium. J. Inorg. Organomet. Polym Mater. **31**, 1859–1876 (2021)
3. O. Akhavan, E. Ghaderi, Toxicity of graphene and graphene oxide nanowalls against bacteria. ACS Nano **4**, 5731–5736 (2010)
4. E. Zaminpayma, P. Nayebi, M. Emami-Razavi, Electronic properties of the interface between metallic doped zigzag graphene and pristine graphene nanoribbons. J. Inorg. Organomet. Polym Mater. **30**, 3694–3701 (2020)

5. L. Feng, L. Wu, X. Qu, New horizons for diagnostics and therapeutic applications of graphene and graphene oxide. Adv. Mater. **25**, 168–186 (2013)

6. D. Plach, J. Jampilek, Graphenic materials for biomedical applications. Nanomaterials **9**, 1758 (2019)

7. G. Lalwani, A. M. Khan, B. Sitharaman, S. Brook, S. Brook, Toxicology of Graphene-Based Nanomaterials. Adv Drug Deliv Rev **105**, 109–144 (2016)

8. C. Liu, J. Zhao, R. Zhang, H. Li, B. Chen, L. Zhang, H. Yang, Multifunctionalization of graphene and graphene oxide for controlled release and targeted delivery of anticancer drugs. Am. J. Transl. Res. **9**, 5197–5219 (2017)

9. A. D. Garg, D. V. Krysko, P. Vandenabeele, P. Agostinis, Hypericin-based photodynamic therapy induces surface exposure of damage-associated molecular patterns like HSP70 and calreticulin. Cancer Immunol. Immunother. **61**, 215–221 (2012)

10. J. Athinarayanan, V. S. Periasamy, K. A. Alatiah, M. A. Ahmed, A. A. Alshatwi, Green fabrication of Co_3O_4 nanoparticle-decorated reduced graphene oxide sheets: evaluation of biocompatibility on human mesenchymal stem cells for biomedical applications. J. Inorg. Organomet. Polym Mater. **27**, 1110–1116 (2017)

11. M. Grodzik, A. Winnicka, In vitro and in vivo effects of graphene oxide and reduced graphene oxide on glioblastoma. Int. J. Nanomed. **10**, 1585–1596 (2015)

12. Y. Chang, S. Yang, J. Liu, E. Dong, Y. Wang, A. Cao, Y. Liu, H. Wang, In vitro toxicity evaluation of graphene oxide on A549 cells. Toxicol. Lett. **200**, 201–210 (2011)

13. M. Georgieva, B. Vasileva, G. Speranza, D. Wang, K. Stoyanov, M. Draganova-filipova, P. Zagorchev, V. Sarafian, G. Miloshev, N. Krasteva, Amination of graphene oxide leads to increased cytotoxicity in hepatocellular carcinoma cells. Int. J. Mol. **21**, 2427 (2020)

14. M. Kutwin, E. Sawosz, S. Jaworski, M. Wierzbicki, B. Strojny, M. Grodzik, M. E. Sosnowska, M. Trzaskowski, A. Chwalibog, Nanocomplexes of graphene oxide and platinum nanoparticles against colorectal cancer Colo205, HT-29, HTC-116, SW480, liver cancer HepG2, human breast cancer MCF-7, and adenocarcinoma LNCaP and human cervical Hela B cell lines. Materials (Basel) **12**, 909 (2019)

15. K. Chen, Y. Huang, J. Chen, Understanding and targeting cancer stem cells: therapeutic implications and challenges. Nat. Publ. Gr. **34**, 732–740 (2013)

16. F. Safdari, H. Raissi, M. Shahabi, M. D. F. T. Zaboli, Calculations and molecular dynamics simulation study on the adsorption of 5-fluorouracil anticancer drug on graphene oxide nanosheet as a drug delivery vehicle. J. Inorg. Organomet. Polym Mater. **27**, 805–817 (2017)

17. J. Yan, T. Zhong, W. Qi, H. Wang, The application of assembled inorganic and organic hybrid nanoarchitecture of prussian blue/polymers/graphene in glucose biosensing. J. Inorg. Organomet. Polym Mater. **25**, 275–281 (2015)

18. S. Zinatloo-Ajabshir, S. AliHeidari-Asil, M. Salavati-Niasari, Simple and eco-friendly synthesis of recoverable zinc cobalt oxide-based ceramic nanostructure as high-performance photocatalyst for enhanced photocatalytic removal of organic contamination under solar light. Sep. Purif. Technol. **267**, 118667 (2017)

19. S. Zinatloo-Ajabshir, S. Ali Heidari-Asil, M. Salavati-Niasari, Recyclable magnetic $ZnCo_2O_4$-based ceramic nanostructure materials fabricated by simple sonochemical route for effective sunlight-driven photocatalytic degradation of organic pollution. Ceram. Int. **47**, 8959–8972 (2021)

20. S. Zinatloo-Ajabshir, M. Sadat Morassaei, M. Salavati-Niasari, Simple approach for the synthesis of $Dy_2Sn_2O_7$ nanostructures as a hydrogen storage material from banana juice. J. Clean. Prod. **222**, 103–110 (2019)

21. S. Moshtaghi, S. Zinatloo-Ajabshir, M. Salavati-Niasari, Nanocrystalline barium stannate: facile morphology-controlled preparation, characterization and investigation of optical and photocatalytic properties. J. Mater. Sci. Mater. Electron. **27**, 834–842 (2016)

22. S. Zinatloo-Ajabshir, M. S. Morassaei, O. Amiri, M. Salavati-Niasari, Green synthesis of dysprosium stannate nanoparticles using *Ficus carica* extract as photocatalyst for the degradation of organic pollutants under visible irradiation. Ceram. Int. **46**, 6095–6107 (2020)

23. S. Zinatloo-Ajabshir, M. Baladi, M. Salavati-Niasari, Enhanced visible-light-driven photocatalytic performance for degradation of organic contaminants using $PbWO_4$ nanostructure fabricated by a new, simple and green sonochemical approach. Ultrason. Sonochem. **72**, 105420 (2021)

24. S. Zinatloo-Ajabshir, N. Ghasemian, M. Mousavi-Kamazani, M. Salavati-Niasari, Effect of zirconia on improving NOx reduction efficiency of $Nd_2Zr_2O_7$ nanostructure fabricated by a new, facile and green sonochemical approach. Ultrason. Sonochem. **71**, 105376 (2021)

25. S. Zinatloo-Ajabshir, M. Mousavi-Kamazani, Effect of copper on improving the electrochemical storage of hydrogen in CeO_2 nanostructure fabricated by a simple and surfactant-free sonochemical pathway. Ceram. Int. **46**, 26548–26556 (2020)

26. M. Mousavi-Kamazani, S. Zinatloo-Ajabshir, M. Ghodrati, One-step sonochemical synthesis of $Zn(OH)_2/ZnV_3O_8$ nanostructures as a potent material in electrochemical hydrogen storage. J. Mater. Sci. Mater. Electron. **31**, 17332–17338 (2020)

27. S. Zinatloo-Ajabshir, Z. Salehi, O. Amiri, M. Salavati-Niasari, Simple fabrication of $Pr_2Ce_2O_7$ nanostructures via a new and eco-friendly route; a potential electrochemical hydrogen storage material. J. Alloys Compd. **791**, 792–799 (2019)

28. C. Donga, S. B. Mishra, A. S. Abd-El-Aziz, A. K. Mishra, Advances in graphene-based magnetic and graphene-based/TiO_2 nanoparticles in the removal of heavy metals and organic pollutants from industrial wastewater. J. Inorg. Organomet. Polym Mater. **31**, 463–480 (2021)

29. D. Bitounis, H. Ali-boucetta, B. H. Hong, D. Min, Prospects and challenges of graphene in biomedical applications. Adv. Mater. **26**, 2258–2268 (2013)

30. S. M. Mousavi, S. A. Hashemi, Y. Ghasemi, M. Amani, A. Babapoor, O. Arjmand, Applications of graphene oxide in case of nanomedicines and nanocarriers for biomolecules : review study. Drug Metab. Rev. **0**, 1–30 (2019)

31. P. D. Harvey, J. Plé, Recent advances in nanoscale metal–organic frameworks towards cancer cell cytotoxicity: an overview. J. Inorg. Organomet. Polym. Mater. (2021). https://doi.org/10.1007/s10904-021-02011-3

32. J. Shen, M. Shi, N. Li, B. Yan, H. Ma, Y. Hu, M. Ye, Facile synthesis and application of Ag-chemically converted graphene nanocomposite. Nano Res. **3**, 339–349 (2010)

33. H. Liu, S. Hu, Y. Chen, S. Chen, Characterization and drug release behavior of highly responsive chip-like electrically modulated reduced graphene oxide – poly (vinyl alcohol) membranes. J. Mater. Chem. **22**, 17311–17320 (2012)

34. Y. Li, Y. Liu, Y. Fu, T. Wei, L. Le Guyader, G. Gao, R. Liu, Y. Chang, C. Chen, The triggering of apoptosis in macrophages by pristine graphene through the MAPK and TGF-beta signaling pathways. Biomaterials **33**, 402–411 (2012)

35. L. Zhang, J. Xia, Q. Zhao, L. Liu, Z. Zhang, Functional graphene oxide as a nanocarrier for controlled loading and targeted delivery of mixed anticancer drugs. Small **6**, 537–544 (2010)

36. J. Liu, L. Cui, D. Losic, Graphene and graphene oxide as new nanocarriers for drug delivery applications. Acta Biomater. **9**, 9243–9257 (2013)

37. K. Yang, S. Zhang, G. Zhang, X. Sun, S. Lee, Z. Liu, Graphene in mice: ultrahigh in vivo tumor uptake and efficient photothermal therapy. Nano Lett. **10**, 3318–3323 (2010)

38. P. Huang, C. Xu, J. Lin, C. Wang, X. Wang, C. Zhang, X. Zhou, S. Guo, Folic acid-conjugated graphene oxide loaded with photosensitizers for targeting photodynamic therapy. Theranostics **1**, 240–250 (2011)

39. E. L. Niero, B. Rocha-Sales, C. Lauand, B. A. Cortez, M. M. de Souza, P. Rezende-Teixeira, M. S. Urabayashi, A. A. Martens, J. H. Neves, G. M. Machado-Santelli, The multiple facets of drug resistance: one history, different approaches. J. Exp. Clin. Cancer Res. **33**, 37 (2014)

40. B. Zhang, P. Wei, Z. Zhou, T. Wei, Interactions of graphene with mammalian cells: Molecular mechanisms and biomedical insights. Adv. Drug Deliv. Rev. **105**, 145–162 (2016)

41. B. F. M. Ribeiro, M. M. Souza, D. S. Fernandes, D. R. do Carmo, G. M. Machado-Santelli, Graphene oxide-based nanomaterial interaction with human breast cancer cells. J. Biomed. Mater. Res. - Part A **108**, 863–870 (2020)

42. N. Chatterjee, H. -J. Eom, Choi, J. , A systems toxicology approach to the surface functionality control of graphene-cell interactions. Biomaterials **35**, 1109–1127 (2014)

43. N. I. Zaaba, K. L. Foo, U. Hashim, S. J. Tan, W. Liu, C. H. Voon, Synthesis of graphene oxide using modified hummers method: solvent influence. Proc. Eng. **184**, 469–477 (2017)

44. A. Bellova, E. Bystrenova, M. Koneracka, P. Kopcansky, F. Valle, N. Tomasovicova, M. Timko, J. Bagelova, F. Biscarini, Z. Gazova, Effect of Fe(3)O(4) magnetic nanoparticles on lysozyme amyloid aggregation. Nanotechnology **21**, 65103 (2010)

45. Q. Yuan, G. Zhou, L. Liao, Y. Liu, L. Luo, Interfacial structure in AZ91 alloy composites reinforced by graphene nanosheets. Carbon N. Y. **127**, 177–186 (2017)

46. M. Kashif, E. Jaafar, P. Bhadja, F. W. Low, S. K. Sahari, S. Hussain, F. K. Loong, A. Ahmad, T. S. AlGarni, M. Shafa et al., Effect of potassium permanganate on morphological, structural and electro-optical properties of graphene oxide thin films. Arab. J. Chem. **14**, 102953 (2021)

47. L. Bokobza, Some applications of vibrational spectroscopy for the analysis of polymers and polymer composites. Polymers (Basel) **11**, 1159 (2019)

48. A. Kołodziej, E. Długoń, M. Świętek, M. Ziąbka, E. Dawiec, M. Gubernat, M. Michalec, A. Wesełucha-Birczyńska, A Raman spectroscopic analysis of polymer membranes with graphene oxide and reduced graphene oxide. J. Compos. Sci. **5**, 20 (2021)

49. R. Muzyka, S. Drewniak, T. Pustelny, M. Sajdak, Ł Drewniak, Characterization of graphite oxide and reduced graphene oxide obtained from different graphite precursors and oxidized by different methods using Raman spectroscopy statistical analysis. Materials (Basel) **14**, 769 (2021)

50. H. Pan, S. Zhu, L. Mao, Graphene nanoarchitectonics: approaching the excellent properties of graphene from microscale to macroscale. J. Inorg. Organomet. Polym Mater. **25**, 179–188 (2015)

51. N. Kurnosov, V. Karachevtsev, Composite films of graphene oxide with semiconducting carbon nanotubes: Raman spectroscopy characterization. Low Temp. Phys. **47**, 206–213 (2021)

52. L. Chang, Y. Cao, W. Peng, C. Li, G. Fan, X. Song, C. Jia, Insight into the effect of oxidation degree of graphene oxides on their removal from wastewater via froth flotation. Chemosphere **262**, 127837 (2021)

53. B. Ossonon, D. Bélanger, Synthesis and characterization of sulfophenyl-functionalized reduced graphene oxide sheets. RSC Adv. **7**, 27224–27234 (2017)

54. N. Pandey, C. Tewari, S. Dhali, B. S. Bohra, S. Rana, S. P. S. Mehta, S. Singhal, A. Chaurasia, N. G. Sahoo, Effect of graphene oxide on the mechanical and thermal properties of graphene oxide/hytrel nanocomposites. J. Thermoplast. Compos. Mater. **34**, 55–67 (2021)

55. S. A. Mousavi, S. Mehrpooya, Fabrication of copper centered metal organic framework and nitrogen, sulfur dual doped graphene oxide composite as a novel electrocatalyst for oxygen reduction reaction. Energy **214**, 119053 (2021)

56. S. M. Bhagyaraj, O. S. Oluwafemi, *Nanotechnology: The Science of the Invisible. Synthesis of Inorganic Nanomaterials* (Elsevier Ltd. , Amsterdam, 2018), pp. 1–18

57. D. Titus, E. J. J. Samuel, S. M. Roopan, *Nanoparticle Characterization Techniques* (Elsevier Inc. , Amsterdam, 2019)

58. S. Zhang, J. Li, G. Lykotrafitis, G. Bao, S. Suresh, Size-dependent endocytosis of nanoparticles. Adv Mater **21**, 419–424 (2009)

59. J. Linares, M. Concepcio, P. A. A. P. Marques, M. T. Portole, Endocytic mechanisms of graphene oxide nanosheets in osteoblasts, hepatocytes and macrophages. ACS Appl. Mater. Interfaces **6**, 13697–13706 (2014)

60. E. Fröhlich, The role of surface charge in cellular uptake and cytotoxicity of medical nanoparticles. Int. J. Nanomed. **7**, 5577–5591 (2012)

61. Q. Yang, W. Zhongying, A. C. E. Owensa, I. Kulaotsa, Y. Chen, A. B. Kane, R. H. Hurt, Antioxidant chemistry of graphene-based materials and its role in oxidation protection technology. Nanoscale **6**, 11744–11755 (2015)

62. M. S. Blois, Antioxidant determinations by the use of a stable free radical. Nature **181**, 1199–1200 (1958)

63. Y. Lee, Y. Yoon, H. Yoon, S. Song, H. Park, Y. Y. Lee, H. Shin, S. W. Hwang, K. Yeum, Enhanced antioxidant activity of bioactives in colored grains by nano-carriers in human lens epithelial cells. Molecules **23**, 1327 (2018)

64. D. Suresh, M. A. P. Kumar, H. Nagabhushana, S. C. Sharma, Cinnamon supported facile green reduction of graphene oxide, its dye elimination and antioxidant activities. Mater. Lett. **151**, 93–95 (2015)

65. R. Rajeswari, H. G. Prabu, Synthesis characterization, antimicrobial, antioxidant, and cytotoxic activities of ZnO nanorods on reduced graphene oxide. J. Inorg. Organomet. Polym. Mater. (2017). https://doi.org/10.1007/s10904-017-0711-9

66. L. Elias, R. Taengua, B. Frígols, B. Salesa, A. Serrano-Aroca, Carbon nanomaterials and led irradiation as antibacterial strategies against gram-positive multidrug-resistant pathogens. Int. J. Mol. Sci. **20**, 3603 (2019)